Design and Real-Time Validation of Higher Order Sliding Mode Observer-Based Integral Sliding Mode MPPT Control for a DC Microgrid
Conception et validation en temps réel d'un contrôle MPPT à mode glissant intégral basé sur un observateur à mode glissant d'ordre supérieur pour un micro-réseau à courant continu

Vijaya Kumar Dunna, Kumar Pakki Bharani Chandra, Pravat Kumar Rout, *Member, IEEE*, and Binod Kumar Sahu, *Member, IEEE*

***Abstract*— In a photovoltaic (PV) system-based microgrid, maximum power point tracking (MPPT) control plays a crucial role to improve the efficiency and stability. Since the past few years, one of the key control schemes to enhance the effectiveness of the microgrid is the observer-based MPPT control. This article proposes a higher order sliding mode observer (HOSMO)-based integral sliding mode control (ISMC) for MPPT control to ensure an efficient operation of a closed-loop dc microgrid. The proposed MPPT control is mainly focused on obtaining a chatter-free output voltage and stabilized output power from the PV-system-based microgrid and further ensure insensitivity to uncertainties and reduction in steady-state error. ISMC is applied to carry out finite-time stabilization throughout the entire response of the system. To justify the efficacy of the proposed approach, various test scenarios are simulated in real-time, and the performance is investigated through extensive comparative results. The MATLAB simulations and real-time simulation results achieved with OPAL-RT are compared. The superior performance of the proposed approach is observed in terms of high efficiency, good accuracy, and robust performance under varying meteorological conditions.**

***Résumé*— Dans un micro-réseau basé sur un système photovoltaïque (PV), le contrôle du point de puissance maximale (MPPT) joue un rôle crucial pour améliorer l'efficacité et la stabilité. Depuis quelques années, le contrôle MPPT basé sur un observateur est l'un des principaux schémas de contrôle permettant d'améliorer l'efficacité du micro-réseau. Cet article propose une commande en mode glissant intégral (ISMC) basée sur un observateur d'ordre supérieur (HOSMO) pour la commande MPPT afin d'assurer un fonctionnement efficace d'un micro-réseau à courant continu en boucle fermée. La commande MPPT proposée est principalement axée sur l'obtention d'une tension de sortie exempte de parasites et d'une puissance de sortie stabilisée à partir du micro-réseau basé sur un système PV, et garantit en outre l'insensibilité aux incertitudes et la réduction de l'erreur en régime permanent. La méthode ISMC est appliquée pour effectuer une stabilisation en temps fini sur l'ensemble de la réponse du système. Pour justifier l'efficacité de l'approche proposée, divers scénarios de test sont simulés en temps réel et les performances sont étudiées à l'aide de résultats comparatifs détaillés. Les simulations MATLAB et les résultats de simulation en temps réel obtenus avec OPAL-RT sont comparés. La performance supérieure de l'approche proposée est observée en termes d'efficacité élevée, de bonne précision et de performance robuste dans des conditions météorologiques variables.**

***Index Terms*— Higher order sliding mode observer (HOSMO), integral sliding mode control (ISMC), maximum power point tracking (MPPT), photovoltaic (PV) systems.**

Manuscript received 8 April 2022; revised 18 July 2022, 25 August 2022, and 23 September 2022; accepted 26 September 2022. Date of publication 13 December 2022; date of current version 19 December 2022. *(Corresponding author: Vijaya Kumar Dunna.)*

Vijaya Kumar Dunna, Pravat Kumar Rout, and Binod Kumar Sahu are with the Department of Electrical Engineering, ITER, Siksha 'O' Anusandhan (Deemed to be University), Bhubaneswar 751030, India (e-mail: vijayakumardunna@gmail.com; pkrout_india@yahoo.com; binodsahu@soa.ac.in).

Kumar Pakki Bharani Chandra is with the Department of Electrical, Electronics and Communication Engineering, and the Center for Autonomous Systems, GITAM (Deemed to be University), Visakhapatnam 530045, India (e-mail: cpakki@gitam.edu).

Associate Editor managing this article's review: Mingxi Liu.

Digital Object Identifier 10.1109/ICJECE.2022.3211470

I. Introduction

RECENTLY, the world is moving on to renewable energy sources due to an increase in energy demand and fuel cost along with alarming situations of global warming and pollution [1]. In renewable energy sources, most of the energy is generated from photovoltaics (PVs) where the initial cost and maintenance are less, along with the free availability of the input solar energy. Solar generationis increased seven times from 2010 to 2020, i.e., approximately 14% of the present generation [2]. However, generating consistent and continuous PV-based power is challenging since it depends

on solar irradiance and the surrounding temperature, both of which can fluctuate arbitrarily and nonlinearly in real-time. The PV system should operate at the maximum power point (MPP) to retrieve the maximum power (MP) available at the input, which is one of the primary concerns that must be addressed to lessen the aforementioned linked operational difficulties. Some MPP tracking (MPPT) control methods were developed as a solution to these associated concerns by identifying the MPP on the P–V characteristic curve and tracking the MP from the solar energy [3]. Using the MPPT control in the PV system, the efficiency and stability of the overall system can be improved. This motivates the present study to investigate further to design a sliding mode control (SMC) to track the MP from the PV network in a microgrid.

In general, the MPPT control systems monitor the PV parameters and generate a control signal to adjust the duty cycle of dc–dc converter switches such that the operating point matches the P–V curve's MPP. An optimal MPPT strategy needs to have the following factors such as [4]: 1) the ability to offer high accuracy and find the correct global MPP for achieving high efficiency; 2) a fast-tracking speed to avoid a drop in extracted power and low efficiency under both uniform and partial shade situations; 3) independent and capable of performing well with a variety of PV systems; 4) simple and straightforward to implement in real-time; 5) must not oscillate around MPP; 6) able to effectively track MPP with the variation in the environmental conditions; and 7) able to reduce the uncertainties and reduction in steady-state error. Different MPPT control methods recently suggested by various authors were categorized and compared in [5] and [6]. Popular traditional control methods include perturb and observe (P&O), hill-climbing, and incremental conductance [7], [8]. These control algorithms are easy to execute, and the low-cost establishment is their major advantage. Sometimes a sudden climatic change, just before reaching the MPP, may introduce an error in the tracking direction, and because of that, the system takes more time to reach the MP extraction point [9], [10]. These limitations make the conventional methods less attractive in rapidly changing the environmental conditions and system uncertainties. Later, as an improvement to reach the MPP in less time, fuzzy-logic-based controllers were introduced for MPPT control for PV systems [11], [12], [13]. A novel adaptive fuzzy-logic-based MPPT control was introduced in [14], which is capable of reaching the MPP in less time and track the MP with nonlinearities at the input source level. However, the major limitation lies in its complex approach to determine the limits of fuzzification and duzzification centers. To reduce this complexity, artificial neural networks (ANN) and optimization algorithms were introduced in [15], [16], and [17]. To improve the precision during sudden changes in climatic conditions, a few optimization techniques [18] were proposed to improve the system efficiency. Under partial shading situations, particle swarm optimization was applied to improve the duty cycle of the converter in [19] and [20]. However, these algorithms use many random variables to optimize the switching signal of the boost converter and are computationally intense. It is essential to design separate robust and efficient MPPT control strategy for specific applications of PV. To overcome these drawbacks, the present research focuses on robust control techniques due to their high reliability, a wide range of stable regions of operation, and higher controllability to efficiently enhance the stability.

SMC for MPPT [7] is one of the most preferred control techniques. A modified form of sliding mode MPPT control was presented and compared in [21]. However, the conventional SMC has a drawback of the high-frequency chattering effect in the output voltage. To handle this problem, an improvised integral SMC (ISMC) was proposed in [22]. A double integral sliding mode (DISM) MPPT and adaptive DISM-MPPT controllers [23], [24] were introduced to improve further tracking performance and reduce the chattering in output voltage. The SMC approach has an immense capability to retrofit with other existing controllers and can be easily combined with observers or state estimators for efficient operation. The foregoing ideas motivate the current research to provide a superior method to adopt SMC that incorporates an integral tracking error term into the existing sliding surface of SMC for a dc microgrid. To enhance the reliability and limit the deployment of maximum number of sensors, many researchers have integrated the estimator or observer to estimate the state variables for plant control. To estimate the disturbance in the system, [25] and [26] introduced a robust observer and second-order sliding mode gradient observer for chatter-free output voltage while concurrently enhancing the tracking speed. When the degree of the variable is equal to two, the second-order sliding modes can make the sliding variables vanish in a finite period. However, one of the major limitations of this approach is when there are some unidentified variables present in the system; it is quite difficult to suppress the high-frequency chattering in the outputs [27]. Second, to save cost and maintenance, state observers must be designed to estimate real-time state vectors, resulting in a reduction in the number of sensors.

In this work, higher order sliding mode observers (HOSMOs) have been designed to address the aforementioned issues by providing accurate observation and guaranteed stability. HOSMOs also suffice distinct control strategies which can be used to nullify the matched uncertainties or disturbances caused by unknown inputs [28]. The integration of disturbance observers to ISMC can reduce the discontinuous control and chatter problem. The initial idea of this work was detailed in [29], which is considered in the proposed approach to carry out all the associated benefits to have a better technique for MPPT control of the PV network. The main contributions of this work are as follows.

1) HOSMO-ISMC-based MPPT control is proposed for a dc microgrid and is compared with the conventional extended Kalman filter (EKF)-based control.
2) The stability of the proposed HOSMO-ISMC for the dc microgrid is derived.
3) Validation of the proposed controller–observer scheme (HOSMO-ISMC) through simulations and in real-time environment using OPAL-RT in nominal and with varying meteorological conditions.

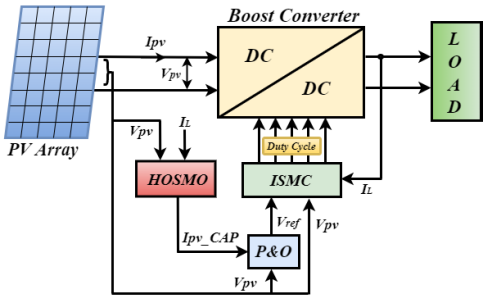

Fig. 1. Block diagram of a PV plant with a proposed combined observer control strategy.

II. System Modeling for Proposed Control Scheme

A. Structure of Plant

The proposed PV-based isolated dc microgrid is implemented using a PV array with the association of a dc–dc boost converter along with the load resistance. The intermediate connections and the proposed controller are presented in Fig. 1. A robust and efficient ISMC based on HOSMO is designed to control the dc–dc converter. The main objective of the HOSMO is to observe and estimate the PV current (I_{pv}) of the plant. By this observation, the PV output power is regulated. The HOSMO takes inductor current (I_L) and PV voltage (V_{pv}) as input parameters from the PV array and boost converter to estimate the desired states. The reference voltage (V_{ref}) is given to the sliding surface presented in ISMC to generate the control signal for the boost converter switch. By controlling the switching of the boost converter, the power tracking performance of the PV system can be regulated.

B. PV Modeling

Fig. 2 represents an equivalent model of a single-diode PV module. The PV array is built using a combination of parallel and series modules. The number of series and parallel modules depend on the rating of the PV panel and the environmental factors such as input energy conditions, temperature, and irradiance. The mathematical equations of the corresponding PV circuit are presented in [30]. The voltage and current values of the PV panel depend on the number of series and parallel modules N_s and N_p, respectively. The mathematical expressions of I_{pv} and V_{pv} are

$$I_{\text{pv}} = N_p i_{\text{pv}}; \quad V_{\text{pv}} = N_s n_s \upsilon_{\text{pv}} \tag{1}$$

and

$$I_{\text{pv}} = N_p I_{\text{ph}} - N_p I_{\text{rs}}\left[\exp\left(\frac{q}{\text{HKT}}\left[\frac{V_{\text{pv}}}{n_s N_s} + \frac{R_s I_{\text{pv}}}{N_p}\right] - 1\right)\right] - \frac{N_p}{R_{\text{sh}}}\left[\frac{V_{\text{pv}}}{n_s N_s} + \frac{R_s I_{\text{pv}}}{N_p}\right] \tag{2}$$

where n_s is the number of series cells, I_{ph} denotes the light-generated current, and I_{rs} is the reverse saturation current. q represents the electronic charge, H is the ideality factor, K is Boltzmann's constant, and T corresponds to the cell temperature. R_s and R_{sh} are the series and shunt resistances of the boost converter, respectively. The presented PV network

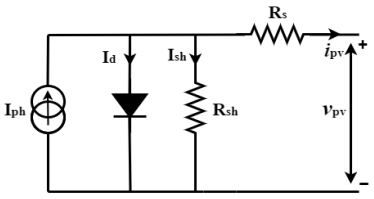

Fig. 2. Single-diode PV circuit [30].

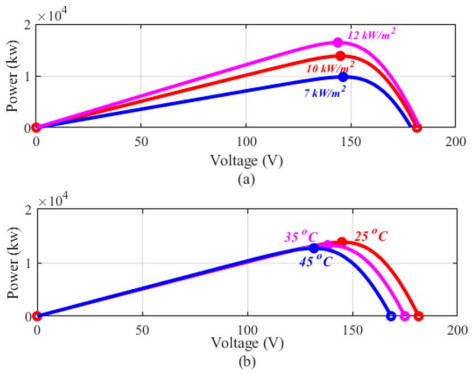

Fig. 3. MPP characteristics of PV array. (a) Specific irradiations. (b) Specific temperatures.

is made up of five series strings, and each string consists of 36 parallel strings. To capture MP from PV array, the PV system should be operated in the MPPT mode. The PV power–voltage relationship for specific irradiations and temperatures is presented in Fig. 3. With the use of a boost converter control signal, the MPPT can be achieved by varying the PV voltage output.

C. Boost Converter Modeling

The purpose of the boost converter is to change a dc voltage level to another to increase the efficiency of the PV system. To increase the PV voltage level, a high-frequency switching signal is needed to turn on and turn off the switch used in the boost converter. The control action is developed for a boost converter that generates a PWM signal to track the power at the MPP. The state equations of the boost converter from Fig. 4 can be represented as follows [24]:

$$\dot{x}_1 = \dot{I}_L = \frac{1}{L}\left[V_{\text{pv}} - \overline{u} V_{\text{dc}}\right]; \quad \dot{x}_2 = \dot{V}_{\text{pv}} = \frac{1}{C_1}\left[I_L - I_{\text{pv}}\right] \tag{3}$$

where $\overline{u} = 1 - u$ is the control signal of the switch, V_{pv} and I_L are the state variables, and I_{pv} is given in (2). For the MPPT operation, the system needs an algorithm to generate the reference operating voltage V_{ref} according to the different operating conditions. The control circuit generates a switching signal, which is then used to obtain the desired PV voltage level by the boost converter.

III. Design and Implementation of Proposed Control Strategy

The P&O algorithm was adopted to generate V_{ref} due to its simplicity in design, low-cost investment, and ease of execution [7]. The algorithm is designed to reduce the

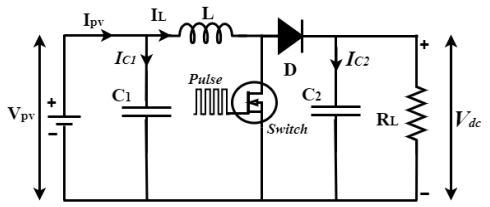

Fig. 4. Boost converter.

perturbation present in the PV output current and voltage due to environmental factors such as variations in irradiation and temperature. The duty cycle of the boost converter needs to be controlled to handle this issue to avoid perturbation in the PV current and output voltage.

A. Design of HOSMO

The suggested HOSMO enables exact direct measurement for n number of derivatives and real-time accurate observation in the presence of measurement noise [31]. To design the HOSMO, the revised states $x_1 = I_L$ and $x_2 = V_{\text{pv}}$ are modified as follows:

$$\begin{aligned} \dot{x}_1 &= \dot{I}_{\text{pv}} = f_1(t, x_1) + \xi(t) \\ \dot{x}_2 &= \dot{V}_{\text{pv}} = f_2(x_2, u); \quad y = x_2 \end{aligned} \tag{4}$$

where $u \in \Re$ is the known input, $y = x_2 \in \Re$ is a measured variable, and $x_1 \in \Re$ is an estimated variable. f_1 is a known discontinuous function, and f_2 is the continuous time function. ξ represents the uncertainty and measurement error caused by the irradiation and temperature deviations. The measurements of PV voltage (V_{pv}) and PV current (I_{pv}) are necessary to generate the reference voltage (V_{ref}) to track MP from PV array. Therefore, I_{pv} is estimated through HOSMO from the measurable states V_{pv} and I_L [32]. The estimated states using HOSMO are

$$\dot{\hat{x}}_1 = \hat{x}_2 + z_1 + \xi; \quad \dot{\hat{x}}_2 = \hat{x}_3 + u + z_2; \quad \dot{\hat{x}}_3 = z_3. \tag{5}$$

Here, z_1–z_3 are the associated correlation terms. Initially, x_3 is assumed as zero at the finite time, and the disturbance ξ is assumed as a Lipschitz and $|\dot{\xi}| < \triangle$. Then the errors $e_1 = x_1 - \widehat{x_1}$ and $e_2 = x_2 - \widehat{x_2}$ are used to compute the correlation terms mentioned as follows:

$$z_1 = \lambda_1 |e_1|^{\frac{2}{3}} \text{sgn}(e_1); \quad z_2 = \lambda_2 |e_1|^{\frac{1}{3}} \text{sgn}(e_1); \quad z_3 = \lambda_3 \text{sgn}(e_1). \tag{6}$$

Here, λ_1–λ_3 are the gains of HOSMO. After a finite time $t > T_2$, the states become $x_1 = \hat{x}_1$ and $x_2 = \hat{x}_2$. The error dynamics can be written as follows:

$$\left.\begin{aligned} \dot{e}_1 &= -\lambda_1 |e_1|^{\frac{2}{3}} \text{sgn}(e_1) + e_2 \\ \dot{e}_2 &= -\lambda_2 |e_1|^{\frac{1}{3}} \text{sgn}(e_1) + e_3 \\ \dot{e}_3 &= -\lambda_3 \text{sgn}(e_1) + \xi(t). \end{aligned}\right\} \tag{7}$$

The finite-time stability analysis of the aforementioned equation is considered from [33] and [34]. The Lyapunov function is

$$\begin{aligned} V_1 = \gamma_1 |e_1|^{\frac{4}{3}} - \gamma_{12} \lfloor e_1 \rceil^{\frac{2}{3}} e_2 + \gamma_2 |e_2|^2 + \gamma_{13} e_1 e_3 \\ - \gamma_{23} e_2 \lfloor e_3 \rceil^2 + \gamma_3 |e_3|^4. \end{aligned} \tag{8}$$

Here, the V_1 is a homogeneous function that is differentiable everywhere. The coefficients $(\gamma_1, \gamma_{12}, \gamma_2, \gamma_{13}, \gamma_{23}, \gamma_3)$ and gains $(\lambda_1, \lambda_2, \lambda_3)$ are selected such that $V_1 > 0$ and $\dot{V}_1 < 0$; and $\gamma_1 > 0$, $\gamma_1\gamma_2 - (1/4)\gamma_{12}^2 > 0$, $\gamma_3[\gamma_1\gamma_2 - (1/4)\gamma_{12}^2] - (1/4)\gamma_{12}^2 > 0$. The derivative of the Lyapunov function (8) along with the trajectories of the perturbed system is

$$\begin{aligned} \dot{V}_1 = &-q_{11}|e_1| + q_{12} \lfloor e_1 \rceil^{\frac{1}{3}} e_2 - \frac{2}{3}\gamma_{12} \frac{|e_2|^2}{|e_1|^{\frac{1}{3}}} - \gamma_{12} \lfloor e_1 \rceil^{\frac{2}{3}} e_3 \\ &+ \gamma_{23} k_2 \lfloor e_1 \rceil^{\frac{1}{3}} \lfloor e_3 \rceil^2 - q_{13} \lfloor e_2 \rceil e_3^3 \\ &+ q_{23} e_2 e_3 - \gamma_{23} |e_3|^3 \end{aligned} \tag{9}$$

where, $q_{11} = ((4/3)\gamma_1 k_1)$, $q_{12} = 2((2/3)\gamma_1 - \gamma_2 k_2 + (1/3)\gamma_{12} k_1)$ $q_{13} = 4\gamma_3(k_3 - \xi(t)\lfloor x_1 \rceil)$ and $q_{23} = 2[\gamma_2 + \gamma_{23}(k_3 - \lfloor x_1 \rceil \xi(t))\lfloor x_1 \rceil \lfloor x_3 \rceil]$ The homogeneous function V_1 is the positive definite and $\dot{V}_1$ is negative definite for every value of perturbation; $\dot{V}_1 = -kV^{(3/4)}$. For $k > 0$, the HOSMO stability has been proven by satisfying the condition $\dot{V}_1 < 0$. After convergence of error in finite time $t > T_2$, the state variables considered are as follows:

$$x_1 = \hat{x}_1; \quad x_2 = \hat{x}_2; \quad \text{and} \quad \hat{x}_3 = \xi(t). \tag{10}$$

B. Design of HOSMO-Based ISMC

The ISMC presented in this article has a modified sliding surface based on current error, voltage error, and integral of voltage error to enhance the tracking efficiency and stability of the system. The relative degree of the sliding surface can be enhanced by adding an integral term, which features bounded chattering. The chattering in the system outputs has reduced due to this bounded chattering. The proposed ISMC considers PV voltage error and inductor current error as two state variables, e_1 and e_2, respectively. The considered third state variable for the proposed approach is integral indefinite of e_2. The errors are

$$e_1 = I_{\text{ref}} - I_L; \quad e_2 = V_{\text{ref}} - \beta V_{\text{pv}}; \quad e_3 = \int \left(V_{\text{ref}} - \beta V_{\text{pv}}\right) dt \tag{11}$$

and

$$I_{\text{ref}} = m\left(V_{\text{ref}} - \beta V_{\text{pv}}\right) \tag{12}$$

where m is the voltage error constant and β represents the feedback network ratio. The ISMC is designed to generate the switching signal of the boost converter. The duty ratio is computed to operate within the limit $0 \leq u \leq 1$. The generated switching operating sequence for the boost converter can be represented as follows:

$$u = \begin{cases} 1, & \text{when } S < 0 \\ 0, & \text{when } S > 0. \end{cases} \tag{13}$$

Here, S is a sliding surface

$$S = \alpha_1 e_1 + \alpha_2 e_2 + \alpha_3 e_3 \tag{14}$$

where α_1–α_3 are the sliding coefficients, respectively. The time derivatives of the sliding surface and error derivatives are

$$\dot{S} = \alpha_1 \dot{e}_1 + \alpha_2 \dot{e}_2 + \alpha_3 \dot{e}_3 \tag{15}$$

$$\dot{e}_1 = \frac{m\beta}{C_1}\left(\hat{I}_{\text{pv}} - I_L\right) - \frac{V_{\text{pv}}}{L} + \frac{V_{\text{dc}}}{L} - \frac{V_{\text{dc}}}{L}u \tag{16}$$

$$\dot{e}_2 = \frac{\beta}{C_1}\left(\hat{I}_{\text{pv}} - I_L\right); \quad \dot{e}_3 = V_{\text{ref}} - \beta V_{\text{pv}} \tag{17}$$

where $\hat{I}_{\text{pv}}$ is the HOSMO estimate of the PV current, and u_{eq} can be obtained by considering $\dot{S} = 0$ at the finite time

$$u_{\text{eq}} = \frac{\beta L}{V_{\text{dc}} C_1}\left(m + \frac{\alpha_2}{\alpha_1}\right)\left(\hat{I}_{\text{pv}} - I_L\right) - \frac{V_{\text{pv}}}{V_{\text{dc}}} + 1 + \frac{\alpha_3 L}{V_{\text{dc}}\alpha_1}\left(V_{\text{ref}} - \beta V_{\text{pv}}\right). \tag{18}$$

The combined stability of the proposed HOSMO-ISMC can be verified by considering the Lyapunov function and its derivative as

$$V_2 = \frac{1}{2}S^2 \quad \text{and} \quad \dot{V}_2 = S\dot{S} < 0. \tag{19}$$

From the aforementioned equation and (13), the boost converter control signal is

$$u = 1 \Rightarrow \dot{S} > 0 \Rightarrow K_1 G + K_2 e_2 < V_{\text{pv}} \tag{20}$$

and similarly

$$u = 0 \Rightarrow \dot{S} < 0 \Rightarrow K_1 G + K_2 e_2 > \left(V_{\text{pv}} - V_{\text{dc}}\right) \tag{21}$$

where $K_1 = (\beta L / V_{\text{dc}} C_1)(m + (\alpha_2/\alpha_1))$, $K_2 = (\alpha_3 L/\alpha_1)$, and $G = (\hat{I}_{\text{pv}} - I_L)$. For $\dot{S} > 0$, the stability condition is $K_1 G_{\min} + K_2 e_{2(\max)} < V_{\text{pv}(SS)}$, and for $\dot{S} < 0$, the stability condition is $K_1 G_{\max} + K_2 e_{2(\min)} > (V_{\text{pv}(SS)} - V_{\text{dc}(\min)})$, where $V_{\text{pv}(SS)}$ is the steady-state voltage of the PV panel, $V_{\text{dc}(\min)}$ is the minimum output voltage of the boost converter, $e_{2(\min)}$ and $e_{2(\max)}$ are the minimum and maximum values of error e_2, respectively, and $G_{\min}$ and $G_{\max}$ are the minimum and maximum values of G, respectively. This results in the proposed HOSMO-ISMC being able to provide stability to the system under disturbances. When compared with the independent performance of ISMC, the observer-based ISMC does not need full state feedback.

IV. Real-Time Implementation With OPAL-RT

The experimental setup used to implement the proposed scheme is shown in Fig. 5. The proposed dc microgrid system's simulation diagram is validated in real-time using the latest OPAL-RT module OP5700 which provides rapid control prototyping (RCP) results to help real-time control development. The real-time accuracy of OPAL-RT is reported in [35]. The RCP/HIL (OP5700) simulator is based on eFPGAsim. The building, loading, and execution process is held through the RT-LAB software. The OPAL-RT simulation model is divided into three blocks named master (SM-HOSMO-ISMC), slave, and console (SC-HOSMO-ISMC). The master subsystem has the existing model to execute, and the slave and console blocks are combined as one subsystem. Fig. 6 depicts the proposed dc microgrid arrangement with the proposed MPPT control strategy.

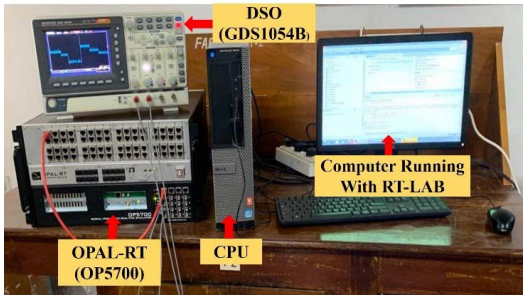

Fig. 5. Experimental block diagram of HOSMO-ISMC with OPAL-RT.

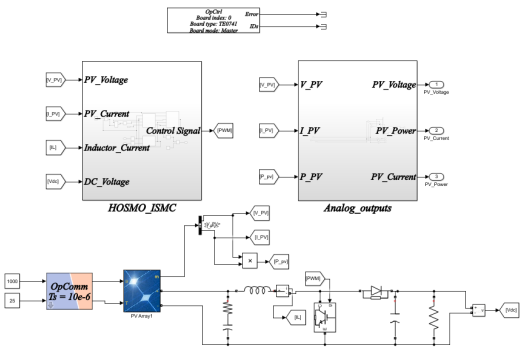

Fig. 6. Subsystem of the master block.

The results are collected from OP5700 using a digital storage oscilloscope (GDS-1054B) through analog output terminals. The boost converter design parameters are taken from [24].

V. Results and Discussion

The comparative results are presented to justify the better performance of the proposed HOSMO-ISMC MPPT control scheme. The standard irradiation of 1000 W/m^2 and temperature of 25 °C are considered in this study. Three different test conditions are simulated by concerning the variations in irradiation, temperature, and load resistance using the proposed approach.

A. Case 1: Comparisons With EKF and STO

In this section, the proposed control strategy's performance is compared with the findings of the advanced estimating techniques EKF and super twisting observer (STO). The designed EKF and STO are adopted from [36] and [37], respectively. The EKF matrices Q and R are tuned based on the sensor noise and process noise. The STO parameters are tuned as in [26] and [37]. Fig. 7 illustrates the proposed control system performance. The results reflect a better performance of the proposed HOSMO-ISMC than EKF and STO. The zoomed-in view of all the results indicates a chatter-free response with less steady-state error.

B. Case 2: Irradiation Change

In this case, the simulation has accomplished the variation in irradiation. By keeping the temperature and load constant, the irradiation is varied from 1000 to 700 and 1200 W/m^2, respectively. The simulation results in Fig. 8 show the impact

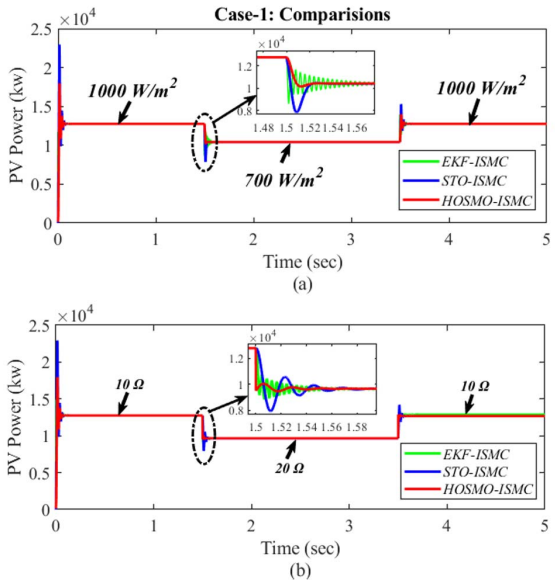

Fig. 7. Comparative analysis of the proposed controller. (a) Irradiation change. (b) Load resistance change.

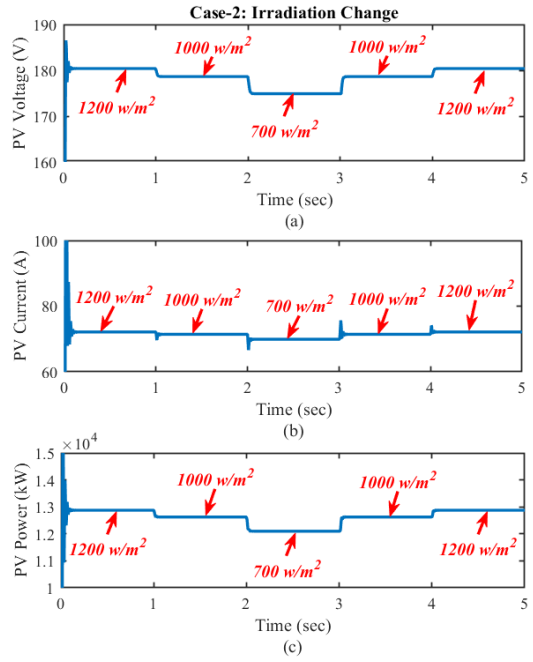

Fig. 8. Output response of the system with irradiation change. (a) PV voltage. (b) PV current. (c) PV power.

of the change in irradiation on the PV plant and boost converter output. The transient response of power, voltage, and current in PV output is stable. By observing the real-time response of the proposed controller, as shown in Fig. 9, it is found that there is a substantial improvement concerning steady-state conditions in comparison to the conventional control techniques.

C. Case 3: Temperature Change

In this case, the test is simulated with a corresponding temperature change, keeping both the irradiation and load constant. The temperature of the PV panel varies from 25 °C to 45 °C, respectively. The simulation results in Fig. 10 show the transient response of the power, voltage, and current for

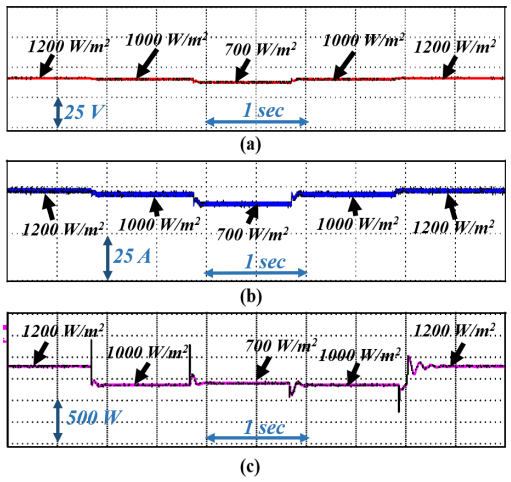

Fig. 9. Real-time output response of the system with irradiation change. (a) PV voltage. (b) PV current. (c) PV power.

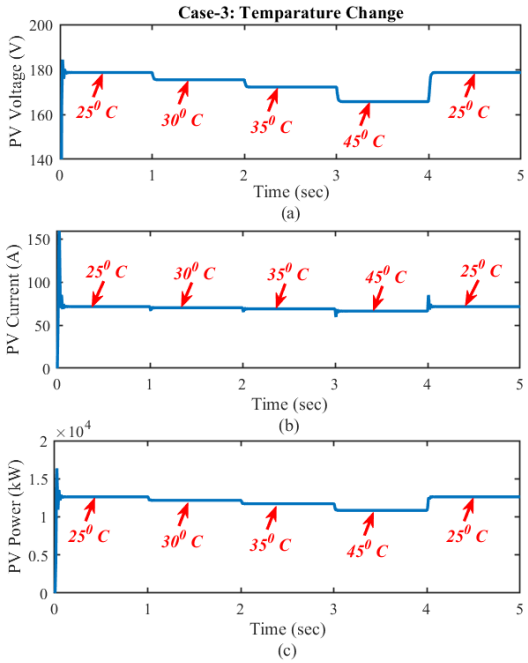

Fig. 10. Output response of the system with temperature change. (a) PV voltage. (b) PV current. (c) PV power.

the PV array. By observing the real-time results presented in Fig. 11, it is found that the proposed control system provides good efficiency and stability even with sudden changes in the temperature level. The proposed control scheme has better results in temperature variation compared with the conventional control techniques of MPPT.

D. Case 4: Load Resistance Change

In this case, the proposed approach is tested with the sudden change in load resistance under constant irradiation and temperature. The load resistance is varied and taken as 10, 25, and 40 Ω, respectively. Figs. 12 and 13 show the response of power voltage and current in PV array under the change in load resistance. The proposed control scheme with MPP yields chatter-free output voltage and stabilized output power under the disturbance that occurred in temperature, irradiation, and load.

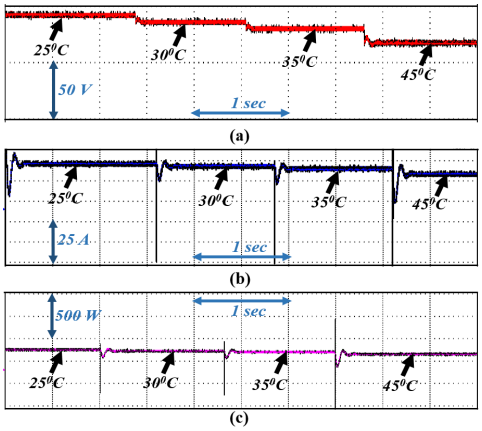

Fig. 11. Real-time output response of the system with temperature change. (a) PV voltage. (b) PV current. (c) PV power.

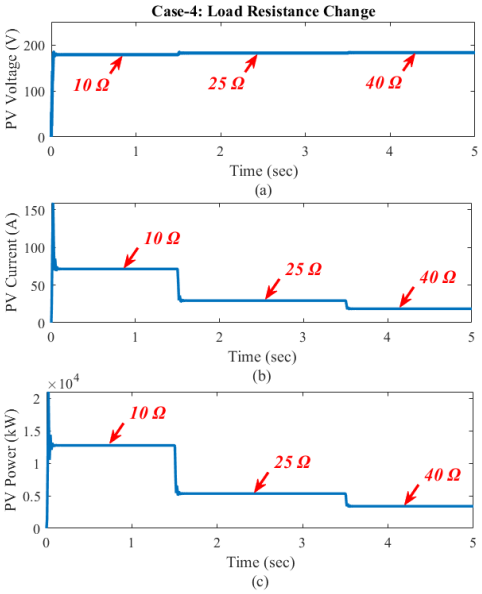

Fig. 12. Output response of the system with load resistance change. (a) PV voltage. (b) PV current. (c) PV power.

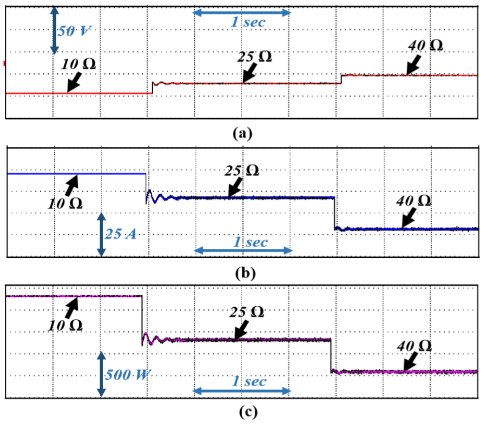

Fig. 13. Real-time output response of the system with load resistance change. (a) PV voltage. (b) PV current. (c) PV power.

VI. Conclusion

The controller design for a dc microgrid based on HOSMO-ISMC is proposed and validated through extensive simulations and real-time simulations under various uncertain conditions. The observer estimates the states with very low estimation error, and the controller ensures dynamically better performance for the closed-loop system due to the integration of the HOSMO with the ISMC controller. The proposed control scheme provides a chatter-free control against uncertain load variations and various environmental conditions. The real-time implementation of HOSMO-ISMC for MPPT control is validated using a real-time simulator OPAL-RT. The results obtained through the conventional and real-time simulations show the efficiency of the proposed control strategy for a dc microgrid model in the presence of varying meteorological conditions.

Acknowledgment

The authors would like to thank GMR Institute of Technology, Rajam, India, for supporting the laboratory facility described in this article.

References

[1] G. Soundarya, R. Sitharthan, C. K. Sundarabalan, C. Balasundar, D. Karthikaikannan, and J. Sharma, "Design and modeling of hybrid DC/AC microgrid with manifold renewable energy sources," *IEEE Can. J. Electr. Comput. Eng.*, vol. 44, no. 2, pp. 130–135, 2021.

[2] A. Al-Enazi, E. C. Okonkwo, Y. Bicer, and T. Al-Ansari, "A review of cleaner alternative fuels for maritime transportation," *Energy Rep.*, vol. 7, pp. 1962–1985, Nov. 2021.

[3] R. A. Mastromauro, M. Liserre, and A. Dell'Aquila, "Control issues in single-stage photovoltaic systems: MPPT, current and voltage control," *IEEE Trans. Ind. Informat.*, vol. 8, no. 2, pp. 241–254, May 2012.

[4] B. Subudhi and R. Pradhan, "A comparative study on maximum power point tracking techniques for photovoltaic power systems," *IEEE Trans. Sustain. Energy*, vol. 4, no. 1, pp. 89–98, Jan. 2013.

[5] A. Mohapatra, B. Nayak, P. Das, and K. B. Mohanty, "A review on MPPT techniques of PV system under partial shading condition," *Renew. Sustain. Energy Rev.*, vol. 80, pp. 854–867, 2017.

[6] F. Liu, Y. Kang, Y. Zhang, and S. Duan, "Comparison of P&O and Hill climbing MPPT methods for grid-connected PV converter," in *Proc. 3rd IEEE Conf. Ind. Electron. Appl.*, Jun. 2008, pp. 804–807.

[7] A. K. Abdelsalam, A. M. Massoud, S. Ahmed, and P. N. Enjeti, "High-performance adaptive perturb and observe MPPT technique for photovoltaic-based microgrids," *IEEE Trans. Power Electron.*, vol. 26, no. 4, pp. 1010–1021, Apr. 2011.

[8] K. S. Tey and S. Mekhilef, "Modified incremental conductance algorithm for photovoltaic system under partial shading conditions and load variation," *IEEE Trans. Ind. Electron.*, vol. 61, no. 10, pp. 5384–5392, Oct. 2014.

[9] L. Piegari and R. Rizzo, "Adaptive perturb and observe algorithm for photovoltaic maximum power point tracking," *IET Renew. Power Gener.*, vol. 4, no. 4, pp. 317–328, Jul. 2010.

[10] A. Safari and S. Mekhilef, "Simulation and hardware implementation of incremental conductance MPPT with direct control method using Cuk converter," *IEEE Trans. Ind. Electron.*, vol. 58, no. 4, pp. 1154–1161, Apr. 2011.

[11] F. Chekired, C. Larbes, D. Rekioua, and F. Haddad, "Implementation of a MPPT fuzzy controller for photovoltaic systems on FPGA circuit," *Energy Proc.*, vol. 6, pp. 541–549, Jun. 2011.

[12] M. M. Algazar, H. Al-Monier, H. A. El-Halim, and M. E. E. K. Salem, "Maximum power point tracking using fuzzy logic control," *Int. J. Electr. Power Energy Syst.*, vol. 39, no. 1, pp. 21–28, 2012.

[13] B. Bendiba, F. Krim, H. Belmili, M. F. Almi, and S. Boulouma, "Advanced fuzzy MPPT controller for a stand-alone PV system," *Energy Proc.*, vol. 50, pp. 383–392, Jun. 2014.

[14] H. Rezk, M. Aly, M. Al-Dhaifallah, and M. Shoyama, "Design and hardware implementation of new adaptive fuzzy logic-based MPPT control method for photovoltaic applications," *IEEE Access*, vol. 7, pp. 106427–106438, 2019.

[15] W. M. Lin, C. M. Hong, and C. H. Chen, "Neural-network-based MPPT control of a stand-alone hybrid power generation system," *IEEE Trans. Power Electron.*, vol. 26, no. 12, pp. 3571–3581, Dec. 2011.

[16] L. M. Elobaid, A. K. Abdelsalam, and E. E. Zakzouk, "Artificial neural network-based photovoltaic maximum power point tracking techniques: A survey," *IET Renew. Power Gener.*, vol. 9, no. 8, pp. 1043–1063, 2015.
[17] S. Messalti, A. Harrag, and A. Loukriz, "A new variable step size neural networks MPPT controller: Review, simulation and hardware implementation," *Renew. Sustain. Energy Rev.*, vol. 68, pp. 221–233, Feb. 2017.
[18] S. Mohanty, B. Subudhi, and P. K. Ray, "A new MPPT design using grey wolf optimization technique for photovoltaic system under partial shading conditions," *IEEE Trans. Sustain. Energy*, vol. 7, no. 1, pp. 181–188, Jan. 2016.
[19] R. B. A. Koad, A. F. Zobaa, and A. El-Shahat, "A novel MPPT algorithm based on particle swarm optimization for photovoltaic systems," *IEEE Trans. Sustain. Energy*, vol. 8, no. 2, pp. 468–476, Apr. 2017.
[20] H. Li, D. Yang, W. Su, J. Lü, and X. Yu, "An overall distribution particle swarm optimization MPPT algorithm for photovoltaic system under partial shading," *IEEE Trans. Ind. Electron.*, vol. 66, no. 1, pp. 265–275, Jan. 2019.
[21] F. F. Ahmad, C. Ghenai, A. K. Hamid, and M. Bettayeb, "Application of sliding mode control for maximum power point tracking of solar photovoltaic systems: A comprehensive review," *Annu. Rev. Control*, vol. 49, pp. 173–196, Jan. 2020.
[22] S.-C. Tan, Y. M. Lai, C. K. Tse, L. Martínez-Salamero, and C.-K. Wu, "A fast-response sliding-mode controller for boost-type converters with a wide range of operating conditions," *IEEE Trans. Ind. Electron.*, vol. 54, no. 6, pp. 3276–3286, Dec. 2007.
[23] R. Pradhan and B. Subudhi, "Double integral sliding mode MPPT control of a photovoltaic system," *IEEE Trans. Control Syst. Technol.*, vol. 24, no. 1, pp. 285–292, Jan. 2016.
[24] B. Subudhi and R. Pradhan, "Adaptive double-integral-sliding-mode-maximum-power-point tracker for a photovoltaic system," *J. Eng.*, vol. 2015, no. 10, pp. 305–317, Oct. 2015.
[25] A. S. Deshpande and S. L. Patil, "Robust observer-based sliding mode control for maximum power point tracking," *J. Control, Autom. Electr. Syst.*, vol. 31, no. 5, pp. 1210–1220, Oct. 2020.
[26] F. Valenciaga and F. A. Inthamoussou, "A novel PV-MPPT method based on a second order sliding mode gradient observer," *Energy Convers. Manag.*, vol. 176, pp. 422–430, Nov. 2018.
[27] S. K. Spurgeon, "Sliding mode observers: A survey," *Int. J. Syst. Sci.*, vol. 39, no. 8, pp. 751–764, Aug. 2008.
[28] Y. Shtessel et al., *Sliding Mode Control and Observation*, vol. 10, 1st ed. New York, NY, USA: Birkhäuser, 2014.
[29] A. Chalanga, S. Kamal, L. M. Fridman, B. Bandyopadhyay, and J. A. Moreno, "Implementation of super-twisting control: Super-twisting and higher order sliding-mode observer-based approaches," *IEEE Trans. Ind. Electron.*, vol. 63, no. 6, pp. 3677–3685, Jun. 2016.
[30] M. N. Ali, K. Mahmoud, M. Lehtonen, and M. M. F. Darwish, "An efficient fuzzy-logic based variable-step incremental conductance MPPT method for grid-connected PV systems," *IEEE Access*, vol. 9, pp. 26420–26430, 2021.
[31] A. Levant, "Higher-order sliding modes, differentiation and output-feedback control," *Int. J. Control*, vol. 76, nos. 9–10, pp. 924–941, 2003.
[32] I.-S. Kim, M.-B. Kim, and M.-J. Youn, "New maximum power point tracker using sliding-mode observer for estimation of solar array current in the grid-connected photovoltaic system," *IEEE Trans. Ind. Electron.*, vol. 53, no. 4, pp. 1027–1035, Jun. 2006.
[33] M. T. Angulo, J. A. Moreno, and L. Fridman, "Robust exact uniformly convergent arbitrary order differentiator," *Automatica*, vol. 49, no. 8, pp. 2489–2495, 2013.
[34] J. A. Moreno, "Lyapunov function for Levant's second order differentiator," in *Proc. IEEE 51st IEEE Conf. Decis. Control (CDC)*, Dec. 2012, pp. 6448–6453.
[35] M. J. Khan, "An AIAPO MPPT controller based real time adaptive maximum power point tracking technique for wind turbine system," *ISA Trans.*, vol. 123, pp. 492–504, Apr. 2022.
[36] A. Sel and C. Kasnakoglu, "Design of extended Kalman filter for SEPIC converter and comparison to Kalman filter," *Social Netw. Appl. Sci.*, vol. 2, no. 4, pp. 1–10, Apr. 2020.
[37] T. Floquet and J. P. Barbot, "Super twisting algorithm-based step-by-step sliding mode observers for nonlinear systems with unknown inputs," *Int. J. Syst. Sci.*, vol. 38, no. 10, pp. 803–815, 2007.

Vijaya Kumar Dunna was born in Andhra Pradesh, India. He received the B.E. degree from the Sir C. R. Reddy College of Engineering, Eluru, India, in 2016, and the M.Tech. degree in power and industrial drives from the GMR Institute of Technology (GMRIT), Rajam, India, in 2019. He is currently pursuing the Ph.D. degree with the Institute of Technical Education and Research, Siksha 'O' Anusandhan (Deemed to be University), Bhubaneswar, India.

He has published a few articles in refereed conferences. His current research interests include control system design and microgrid control applications.

Kumar Pakki Bharani Chandra received the Ph.D. degree from the University of Leicester, Leicester, U.K., in 2013.

He was a Post-Doctoral Research Fellow with the University of Exeter, Exeter, U.K., from 2013 to 2016, after which he held a position of a Professor and the Head of the Department of Electrical and Electronics Engineering, GMR Institute of Technology, Rajam, India, till 2021. He is currently a Professor of Electrical, Electronics and Communication Engineering (EECE) and the Director of the Center for Autonomous Systems, GITAM (Deemed to be University), Visakhapatnam, India. His areas of research include control systems design, state estimation, and artificial organs.

Pravat Kumar Rout (Member, IEEE) received the M.E. degree from Madurai Kamaraj University, Madurai, India, in 1995, and the Ph.D. degree from the Biju Patnaik University of Technology, Rourkela, India, in 2010, all in electrical engineering.

He is currently a Professor with the Department of Electrical and Electronics Engineering, Institute of Technical Education and Research, Siksha 'O' Anusandhan (Deemed to be University), Bhubaneswar, India. He has authored or coauthored hundreds of his research articles in reputed international journals. His research interests include power system protection and control, smart grid, and microgrid applications.

Binod Kumar Sahu (Member, IEEE) received the AMIE degree in electrical engineering from the Institution of Engineers, Kolkata, India, in 2001, the M.Tech. degree from the National Institute of Technology (NIT), Warangal, India, in 2003, and the Ph.D. degree from Siksha 'O' Anusandhan (SOA, Deemed to be University), Bhubaneswar, India, in 2016.

He is currently a Professor with ITER, SOA. His research interests include automatic generation control, fuzzy-logic-based control, soft computing techniques, and time series forecasting.

Dr. Sahu is a member of IET since 2014.